

THE POSITRON SOURCE

H. Brechna, K. E. Breymayer, K. G. Carney,
H. DeStaebler, R. H. Helm, and C. T. Hoard

The purpose of this chapter is to describe the positron source and all its associated subsystems. Following the introduction, the chapter is divided into three major parts: (1) a discussion of general design considerations including the radiator, the focusing system, and predicted yields; (2) a description of the system including the various radiators, the focusing magnets, and special instrumentation and controls; and (3) a summary of early operating experience.

16-1 Introduction (HDeS)

The positron beam at SLAC is generated by a technique similar to that used at other electron linacs.^{1,2} An electron beam is accelerated in the first third of the machine and, at an energy of about 5 GeV, it strikes a radiator located on the axis of the machine. The radiator is several radiation lengths thick. A small fraction of the positrons emerging from the radiator is focused and accelerated in the remaining two-thirds of the machine in which the RF phase is shifted by about 180°. The positron beam is characterized by a maximum energy which is two-thirds of the maximum electron beam energy, by an intensity which is a small percentage of the intensity of the electron beam striking the radiator, and by a transverse phase space which is much larger than that of the usual electron beam. In fact, the phase space is about the maximum that the machine will transmit, 0.15π (MeV/c)(cm).

The SLAC system differs from other positron systems largely because of the high power available in the incident electron beam (up to several hundred kilowatts) and the high energies involved. The high power gives rise to severe thermal problems, both pulsed and steady-state and also to significant radiation problems. Levels on the order of 10^7 rad/hour are anticipated near the radiator

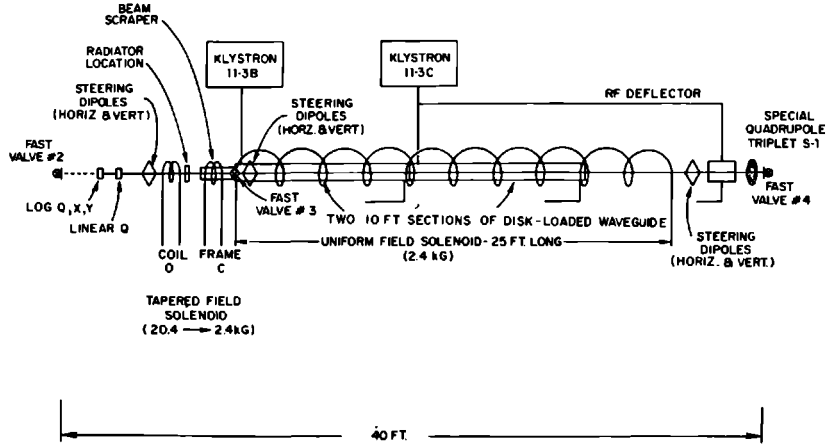
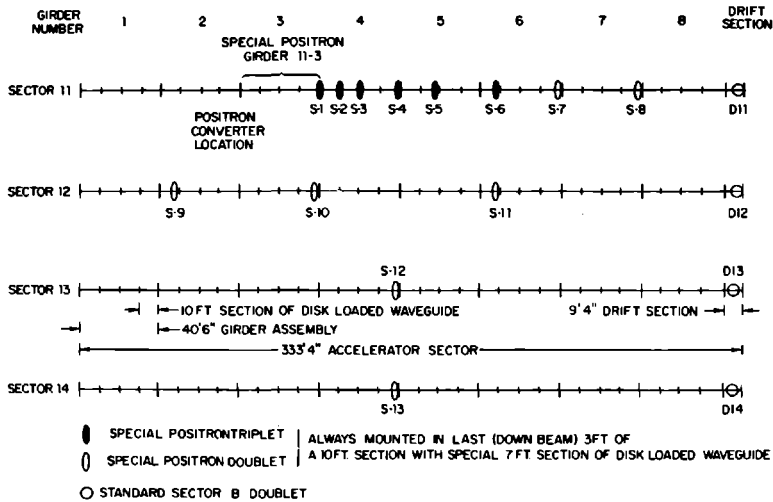


Figure 16-1 Positron source overall layout.

834A1

when it is in use at full beam power, and residual radiation levels of 10 rad/hour have frequently been encountered in early operation at about one-tenth of full power. Since the incident electron beam has an energy of 5 to 6 GeV, the radiator should have a thickness about equal to the shower maximum at this level; in copper, for example, this thickness is several inches. The system that has been built has a wide positron energy acceptance. Such a system seemed promising because the initial energy spread of the positrons at the source

Figure 16-2 Positron focusing system layout.



834A2

(typical useful range between 5 and 15 MeV) becomes unimportant at the end of the machine in relative value, when the positrons emerge at energies of several gigaelectron volts.

The decision to locate the radiator one-third of the way from the injector was rather arbitrary. It represented a compromise between the conflicting desires of high positron intensity, which requires high electron power incident on the radiator, and high final positron energy, which requires that the radiator be placed toward the front end of the accelerator. The experimental uses anticipated for the positron beam were for the scattering of positrons on protons, for a monochromatic photon beam arising from positron–electron annihilation, and possibly for injecting into a positron–electron storage ring.

Figures 16-1 and 16-2 show a layout of the major in-line elements in the positron source system.

16-2 General design considerations

Radiator (HDeS)

The basic design of the radiator is conditioned by the development of the electromagnetic cascade shower. The rate at which energy is absorbed determines the thermal problems. The positron distribution in energy, angle, and transverse position determines the source emittance for the positron beam.

All present SLAC radiators are being made of copper. Preliminary considerations indicated that materials with a large atomic number, Z , would be best, but in such materials the specific heat is low and the linear dimensions are small so that the heating problems are very severe. Furthermore, the positron yield at 0° from copper is only about 20% less than that from lead. The positron yield per incident electron is approximately proportional to the electron energy so that the positron current is proportional to the incident power.

The rate of energy deposition in copper according to a one-dimensional Monte Carlo calculation is shown in Fig. 16-3.³ The incident electron beam is typically 1 mm in diameter, and near shower maximum the effective radius is 2 or 3 mm.⁴ An elementary and approximate steady-state heat transfer calculation for a “slug” radiator suggests that it should melt in the neighborhood of 100-kW incident power.⁵ Under test conditions, one “slug” melted between 120 and 140 kW,⁵ and this empirical knowledge is guiding the design of future solid copper radiators.

The maximum azimuthal and radial thermal stresses, $(\sigma_\theta)_{\max}$ and $(\sigma_r)_{\max}$, arising from one pulse may be estimated from the formulas derived for a thin circular plate:

$$(\sigma_\theta)_{\max} = -(\sigma_r)_{\max} = \frac{E\alpha \Delta T_p}{2} \quad (16-1)$$

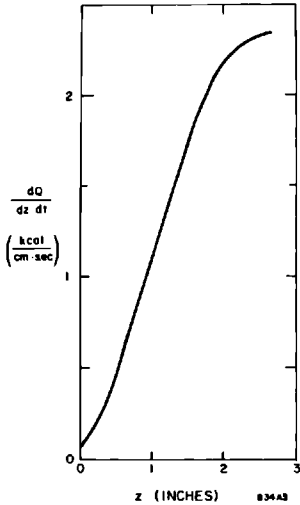


Figure 16-3 Heat deposition as a function of depth for 100 kW of 5-GeV electrons incident on copper.

where E is Young's modulus, α is the coefficient of thermal expansion, and ΔT_p is the temperature rise accompanying one beam pulse. This temperature rise is approximately

$$\Delta T_p = \frac{1}{\rho C_p \pi a^2} \frac{dQ}{dz dt} \frac{1}{v} \quad (16-2)$$

where

ρ = the density ($\rho = 8.9$ for copper)

C_p = the specific heat (0.09 cal/g°C for copper)

a = the radius of energy deposition (3 mm)

$dQ/(dz dt)$ = the rate of heat deposition from Fig. 16-3

v = the accelerator repetition rate (360 pulses/sec)

For an incident beam of 100 kW,

$$\Delta T_p = 27^\circ\text{C/pulse}$$

and

$$\sigma_{\max} = 3600 \text{ psi}$$

which is near the tensile strength for OFHC copper at high temperature (700°C). This implies that cyclic fatigue failure may take place. So far, no failure has been observed after limited operation at 30 to 40 kW.

A liquid radiator was also considered. It has various conceptual advantages but, at present, the accompanying practical uncertainties and complexities seem to outweigh the advantages. In general, experience at SLAC has indicated

Table 16-1 Measured positron yields

E_0 (in GeV, e^-)	Material	Thickness (in radiation lengths)	$\frac{dn}{E_0 dP d\Omega}$ e^+ (in $\frac{1}{(\text{GeV}, e^-)(\text{MeV}/c) \cdot \text{Steradian}}$)	Reference
0.22	Lead	Optimum (1.7)	0.22	Orsay (Ref. 6)
0.165	Lead	Optimum (1.7)	0.22	Orsay (Ref. 6)
1.0	Lead	2.9	0.175	SLAC (Ref. 7)
1.0	Copper	3.0	0.143	SLAC (Ref. 7)

that simplicity, ruggedness, and reliability are preferable to a sophisticated, nonconservative design even though such a design may promise somewhat higher performance.

The detailed distribution in energy, angle, and transverse position of positrons from the radiator is not known very well. It is difficult to compute, even by Monte Carlo techniques, because there are so many variables. A useful quantity that has been measured is the specific positron yield at zero degrees, that is, the number of positrons per steradian at 0° per million electron volt (E) of positron energy per incident electron of energy $E_0(\text{GeV})$. The measured yields are given in Table 16-1. The SLAC yields may be slightly low because of excessive multiple scattering. They dropped somewhat for angles greater than zero; they were fairly constant for E from 5 to 16 MeV but dropped at 35 MeV. The Orsay yields peaked around E equal to 10 to 15 MeV.

Calculated yield (HDeS)

A calculation of the yield of positrons at the end of the machine depends on the beam transport properties of the focusing system of the accelerator as well as on the source emittance. In principle, the beam transport could be calculated; however, at present, there is insufficient information about the five-dimensional source emittance. The five variables are the position and momentum in both transverse directions, and the longitudinal momentum (or total energy divided by c which nearly equals the longitudinal momentum). However, a rough estimate of the yield may be obtained using simple approximations of both the beam transport and the source emittance.

An approximation of the source emittance is obtained by integrating separately over the positron beam cross section, the transverse momentum, and the longitudinal momentum. The integration over cross section is done, effectively, by using the specific yield measured at 0° . The maximum value of transverse momentum at the source that is transmitted is about $0.5 \text{ MeV}/c$. This number may be estimated by noting that the product of maximum transverse momentum and maximum transverse displacement is constant throughout the accelerator, with numerical value $0.15 (\text{MeV}/c)(\text{cm})$, and that an

approximate value for the source radius is 0.3 cm. It seems reasonable to make a rough correction for the way the multidimensional source emittance is handled. The volume of a four-dimensional ellipsoid is $(\pi^2/2)(abcd)$, where a, b, c, d are the semi-axes. The integration over cross section is done as if the area were πab , so that the integration over angle should contain the extra factor of $\frac{1}{2}$, $(\pi/2)cd$. A reasonable range of longitudinal momentum is 6–11 MeV/c because this initial energy spread by itself would give rise to a spread in RF phase angle leading to a final energy spread equal to 0.75% (full width), and it is plausible to assume that general machine operation would broaden this to 1%.

Based on these assumptions, the yield can be calculated as follows:

$$\begin{aligned} \frac{n}{E_0} &= f \int_{P_1}^{P_2} dP \int_0^{p/P} \frac{dn}{E_0 dP d\Omega} 2\pi\theta d\theta \\ &\approx f\pi \left(\frac{dn}{E_0 dP d\Omega} \right) \int_{P_1}^{P_2} \left(\frac{p}{P} \right)^2 dP \\ &= f\pi p^2 \left(\frac{dn}{E_0 dP d\Omega} \right) \left(\frac{1}{P_1} - \frac{1}{P_2} \right) \end{aligned} \quad (16-3)$$

Numerically, one obtains

$$\frac{n}{E_0} = 4.5 \times 10^{-3} e^+ \quad \text{into} \quad 1\%/\text{GeV incident } e^-$$

where

- $f = 0.5$ is the correction factor for the four-dimensional phase space
- $dn/E_0 dP d\Omega = 0.15 e^+/\text{GeV (MeV/c) steradian}$ is the measured specific yield at 0°
- $p = 0.5 \text{ MeV/c}$ is the maximum acceptable transverse momentum
- $P_1, P_2 = 6 \text{ MeV/c}, 11 \text{ MeV/c}$ are the limits of the acceptable longitudinal momentum

Thus, the estimated specific yield, which is probably an upper limit, is 4.5×10^{-3} positron in a final energy width of 1%/GeV of an incident electron; this number is about 3 times larger than the observed yield.

It is interesting to note that a broad phase spectrum can still give a rather sharp energy spectrum although perhaps of low intensity. For example, if the number of positrons per unit RF phase angle is $dn/d\phi$, then the number per unit final energy is

$$\frac{dn}{dE} = \frac{d\phi}{dE} \frac{dn}{d\phi} = -(E_{\max}^2 - E^2)^{-1/2} \frac{dn}{d\phi} \quad (16-4)$$

where

$$E = E_{\max} \cos \phi$$

For constant $dn/d\phi$ (the least favorable case)

$$n = \int_E^{E_{\max}} \frac{dn}{dE} dE = \frac{dn}{d\phi} \int_0^{\cos^{-1}(E/E_{\max})} d\phi = \left(\cos^{-1} \frac{E}{E_{\max}} \right) \frac{dn}{d\phi} \\ \approx \left[2 \left(1 - \frac{E}{E_{\max}} \right) \right]^{1/2} \frac{dn}{d\phi} \quad \text{for } \frac{E}{E_{\max}} \approx 1 \quad (16-5)$$

This formula shows that the particle density per unit energy interval is maximum close to the crest. Thus, for example, 45% of the beam that is within 5% of E_{\max} is actually within 1% of this energy.

Focusing (RHH)

GENERAL PROPERTIES. The positron focusing system functions as a phase-space transformer between the low-energy and large transverse momentum particles emitted by the radiator, and the transport systems of the accelerator and beam switchyard (BSY) which have admittances characterized by small transverse momentum acceptance even at high beam energies.

Table 16-2 lists some parameters relevant to the SLAC positron transport system. The arbitrary design admittance of 0.15π (MeV/c)(cm) is a reasonable compromise between positron yield and the admittance limitations of the BSY and accelerator.

Note that the BSY admittance is compatible with the design admittance at momenta down to $P \approx 2$ GeV/c. The admittance of the accelerator transport system becomes 0.15π (MeV/c)(cm) at a momentum of about 2.5 GeV/c, or four sectors of acceleration; this means that special focusing provisions are required for about four sectors following the positron radiator.

Table 16-2 Parameters affecting positron transport design

Beam switchyard (A-beam) ^a	
Vertical (y) admittance ^b	$0.7\pi P \times 10^{-4}$
Horizontal (x) admittance	$1.15\pi P \times 10^{-4}$
Accelerator (sector doublets) ^c	
Admittance (x and y)	$0.6\pi P \times 10^{-4}$
Radial aperture	0.85 cm
Radiator emittance	
Typical transverse momentum	~ 15 MeV/c
Inherent shower radius (normal density Cu radiator)	~ 1 mm
Typical source radius (dependent on focusing of e^- beam)	1–3 mm
Nominal design admittance for positron transport	0.15π (MeV/c)(cm)

^a See Chapter 17 for details of BSY design. B-beam admittances are approximately a factor of 2 greater than A-beam admittances.

^b Admittances are expressed as phase ellipse areas in units of (MeV/c)(cm), where P , the longitudinal momentum, is expressed in MeV/c.

^c See Chapter 7 for details of accelerator transport system.

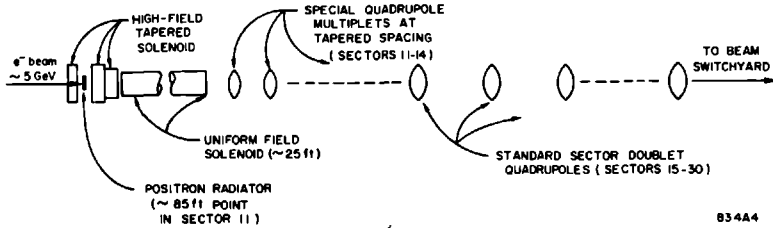


Figure 16-4 Schematic diagram of positron transport components.

Figure 16-4 illustrates schematically the overall layout of positron transport components. Briefly, the operation is as follows: the high-field tapered solenoid transforms the large divergence, small radius emittance at the radiator into a more nearly parallel beam at somewhat larger radius. The uniform-field solenoid then holds the beam together through several accelerator sections, until the energy is high enough for injection into a system of quadrupole lenses at finite spacing. The spacing of the quadrupole lenses tapers up approximately in proportion to the increasing beam energy, thereby maintaining constant admittance, until a match in the standard (sector doublet) focusing system is attained.

SHORT-RANGE FOCUSING—SOLENOIDS. First, a short digression will be made to review briefly the beam optical properties of a solenoidal magnetic field.⁸⁻¹¹ Consider the solenoid to have cylindrical symmetry about the z axis, in which case the field is derivable from a vector potential given by

$$\begin{aligned}
 A_r = A_z &= 0 \\
 A_\phi &= J_1 \left(r \frac{d}{dz} \right) \int_{-\infty}^z B(z_1) dz_1 \\
 &= \frac{1}{2} r B(z) - \frac{1}{16} r^3 B''(z) + \dots
 \end{aligned}
 \tag{16-6}$$

where the “prime” denotes differentiation with respect to z ;

$$\mathbf{B} = \nabla \times \mathbf{A}
 \tag{16-7}$$

and $B(z)$ is the z component of \mathbf{B} evaluated along the z axis.

The general equation of motion*

$$m \frac{d}{dt} (\gamma \mathbf{v}) = e \mathbf{v} \times \mathbf{B}
 \tag{16-8}$$

may be rewritten in terms of the canonical momentum \mathbf{p} :

$$\mathbf{p} = m\mathbf{v} + e\mathbf{A}$$

$$\frac{d\mathbf{p}}{dt} = e\nabla(\mathbf{v} \cdot \mathbf{A})
 \tag{16-9}$$

* Gaussian units with $c = 1$ are used throughout this paragraph.

The well-known invariance of the canonical angular momentum, which results from the cylindrical symmetry of A , may be expressed as

$$p_\phi = xp_y - yp_x = \text{constant} \quad (16-10)$$

Assuming that the motion is predominantly in the $+z$ direction and that the transverse momentum is much smaller than the longitudinal momentum, we can write the equations of motion in *first-order paraxial* expansion, using Eqs. (16-6) and (16-9):

$$\begin{aligned} p'_x &= (Px' - \frac{1}{2}eBy)'\ = \frac{1}{2}eBy' \\ p'_y &= (Py' + \frac{1}{2}eBx)'\ = -\frac{1}{2}eBx' \end{aligned} \quad (16-11)$$

where the scalar momentum is

$$\begin{aligned} P &= m(\dot{y}^2 - 1)^{1/2} \\ &\approx p_z \text{ (first-order approximation)} \\ &\approx m\gamma \text{ (for relativistic electrons or positrons)} \end{aligned}$$

A useful simplification is found by transforming the above equations into a rotating coordinate system (ξ, η) (see Fig. 16-5), where the angle of rotation is the Larmor angle

$$\mu = \frac{1}{2} \int \frac{eB}{P} dz \quad (16-12)$$

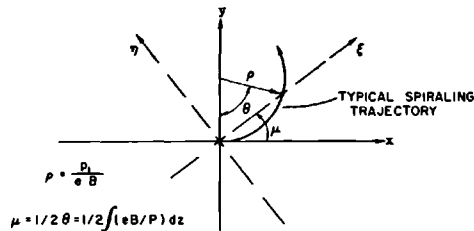
The transformation in four-dimensional phase space is

$$\begin{bmatrix} \xi \\ p_\xi \\ \eta \\ p_\eta \end{bmatrix} = \begin{bmatrix} \cos \mu & 0 & \sin \mu & 0 \\ 0 & \cos \mu & 0 & \sin \mu \\ -\sin \mu & 0 & \cos \mu & 0 \\ 0 & -\sin \mu & 0 & \cos \mu \end{bmatrix} \begin{bmatrix} x \\ p_x \\ y \\ p_y \end{bmatrix} \quad (16-13)$$

and the equations of motion become simply

$$\begin{aligned} p'_\xi &= (P\xi)'\ = -\frac{1}{4} \frac{e^2 B^2}{P} \xi \\ p'_\eta &= (P\eta)'\ = -\frac{1}{4} \frac{e^2 B^2}{P} \eta \end{aligned} \quad (16-14)$$

Figure 16-5 Definition of rotating coordinate system (ξ, η) .



i.e., in the rotating coordinate system, the ξ and η motions are decoupled and are expressed by the differential equation of a simple linear oscillator. Thus, the essential properties of solenoid optics may be described in terms of a one-dimensional motion.

If the parameter $B(z)$ is slowly varying, one may employ the well-known WKB approximation for the solution of Eq. (16-14); the result is

$$\begin{bmatrix} \xi \\ p_\xi \end{bmatrix} = \begin{bmatrix} \left(\frac{B_i}{B}\right)^{1/2} \cos \mu & \frac{2 \sin \mu}{e(B_i B)^{1/2}} \\ -\frac{1}{2}e(B_i B)^{1/2} \sin \mu & \left(\frac{B}{B_i}\right)^{1/2} \cos \mu \end{bmatrix} \begin{bmatrix} x_i \\ p_{xi} \end{bmatrix} \quad (16-15)$$

where the subscript i denotes initial values, $\mu(z_i) = 0$ so that $x_i = \xi_i$ and $p_{xi} = p_{\xi i}$. The result for (η, p_η) is analogous. It may be shown that a sufficient condition for validity of the WKB approximation is

$$|B'| \ll |\mu' B|$$

or

$$(16-16)$$

$$\left| \frac{B'}{B^2} \right| \ll \frac{e}{2P}$$

The transformation in (x, p_x, y, p_y) space may be found from Eqs. (16-13) and (16-15),

$$\begin{bmatrix} x \\ p_x \\ y \\ p_y \end{bmatrix} = \mathbf{R}^{-1} \begin{bmatrix} \mathbf{A} & \mathbf{O} \\ \mathbf{O} & \mathbf{A} \end{bmatrix} \begin{bmatrix} x_i \\ p_{xi} \\ y_i \\ p_{yi} \end{bmatrix} \quad (16-17)$$

where \mathbf{R} is the 4×4 rotation matrix in Eq. (16-13), and \mathbf{A} is the 2×2 matrix in Eq. (16-15).

It can be shown from Eq. (16-15) that the quantity

$$I_2 \equiv \frac{1}{2}eB\xi^2 + \frac{2}{eB} p_\xi^2 \quad (16-18)$$

is conserved along a given trajectory if Eq. (16-16) holds, i.e., I_2 is an *adiabatic invariant*. The area enclosed by this elliptical phase orbit is

$$u \equiv \pi I_2 = \pi \left(\frac{1}{2} eB\xi^2 + \frac{2}{eB} p_\xi^2 \right) \quad (16-19)$$

Similarly, it may be shown from Eq. (16-17) that

$$I_4 \equiv \frac{1}{2}eB(x^2 + y^2) + \frac{2}{eB} (p_x^2 + p_y^2) = \frac{1}{2}eB(\xi^2 + \eta^2) + \frac{2}{eB} (p_\xi^2 + p_\eta^2) \quad (16-20)$$

is conserved. Another invariant function may be found by combining Eqs. (16-10) and (16-20):

$$\begin{aligned}
 J_4 &\equiv I_4 - 2p_\phi \\
 &= \frac{2}{eB} P^2(x'^2 + y'^2) \equiv \frac{2}{eB} p_1^2
 \end{aligned}
 \tag{16-21}$$

It follows from Eq. (16-19) that the maximum (ξ, p_ξ) or (η, p_η) admittance of an adiabatically tapered solenoid of uniform radial aperture, a , is

$$U = \frac{\pi}{2} eB_{\min} a^2
 \tag{16-22}$$

where B_{\min} is the minimum value of B within the solenoid. The maximum initial transverse size and momentum which can be contained are

$$(x_i)_{\max} = \left(\frac{B_{\min}}{B_i}\right)^{1/2} a
 \tag{16-23}$$

$$(p_{xi})_{\max} = \frac{1}{2} e(B_i B_{\min})^{1/2} a
 \tag{16-24}$$

A fundamental limitation on the final energy spectrum of accelerated positrons is imposed by RF debunching caused by differences in transit time. If one neglects the bunching forces in the RF accelerating field, then to second order in the dynamic variables the relative phase slip is given by

$$\delta\phi = \omega \delta t \approx \frac{\pi}{\lambda} \int \left(\frac{1}{\gamma^2} - \frac{1}{\Gamma^2}\right) dz + \frac{\pi}{2\lambda} J_4 \frac{e}{m^2} \int \frac{B}{\gamma^2} dz + \dots
 \tag{16-25}$$

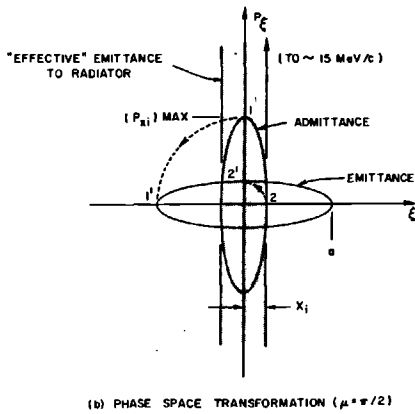
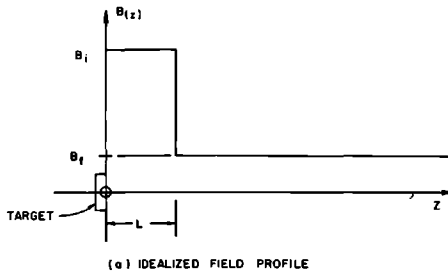
where $m\Gamma$ is a reference energy, λ is the RF wavelength, and J_4 is the invariant function defined by Eq. (16-21).* Here the first term represents the effect of different velocities, and the second term represents the second-order path-length differences of trajectories with finite transverse phase space.

The above formulation can now be applied to actual design concepts. Two types of systems will be described: the "quarter-wave transformer" and the "tapered field solenoid."

Several existing or proposed positron facilities† use the "quarter-wave transformer" principle, so called because of its analogy with transmission line theory. Figure 16-6 illustrates the idealized operation of this type of system. The low-field region, B_f , is assumed to extend along a finite fraction of the accelerator, while the high-field region, B_i , which performs the matching function, turns out to be only a few centimeters long, as shown in Fig. 16-6a. In the phase-space diagram [Fig. 16-6b], the shaded area represents the "effective" radiator emittance, or region which is filled more or less uniformly with positrons. The erect ellipse (admittance) represents the accepted phase

* It may be shown that the limiting values of J_4 are 0 and $2U/\pi$.

† For example, linacs such as those at Frascati, DESY, and Saskatchewan, designed to give low or medium energy positrons.



B34A6

Figure 16-6 Illustration of the quarter-wave transformer principle ($\mu = \pi/2$) in positron matching.

space as seen at the radiator. The flat ellipse (emittance) represents the phase space accepted by the low-field region. The dashed curves 1-1' and 2-2' represent typical phase orbits through the high-field region ($\mu = \pi/2$).

The following relations represent optimum conditions for the quarter-wave transformer:

admittance

$$U = \frac{\pi}{2} e B_f a^2 \tag{16-26}$$

initial field strength

$$B_i = \frac{a}{x_i} B_f \tag{16-27}$$

effective length for $\mu = \pi/2$

$$L = \frac{\pi m \Gamma}{e B_i} \tag{16-28}$$

where a is the limiting aperture, x_i is the effective source width at the radiator, and $m\Gamma$ is the energy for which $\mu = \pi/2$. The energy spread that is satisfactorily matched, i.e., the bandwidth, is estimated as

$$\frac{\Delta\gamma}{\Gamma} \approx C \frac{B_f}{B_i} \quad (16-29)$$

where C is a geometric constant of order unity. The above relations are best illustrated by taking a numerical example. Using $U = 0.3\pi$ (MeV/c)(cm), $a = 0.95$ cm, $x_i = 0.2$ cm, and $m\Gamma = 8$ MeV, one obtains $B_f = 2.2$ kG, $B_i = 10.5$ kG, $L = 8$ cm, and $\Delta\gamma/\Gamma \approx 0.2$. The maximum transverse momentum captured from the radiator is $(p_{xi})_{\max} = 1.5$ MeV/c, which, as assumed, is less than the effective transverse momentum at the radiator. The RF debunching through the high-field region is estimated to be about 0.2° from the velocity spread, the first term of Eq. (16-25), and about 2° from the phase-space-dependent term. Additional debunching in the low-field region will depend on how far the beam drifts before entering the accelerating field but will tend to be small because of the small value of $\Delta\gamma/\Gamma$.

The SLAC positron system makes use of a somewhat different initial matching scheme in that it has an adiabatically tapered solenoid rather than a quarter-wave transformer. The principle of the tapered solenoid may be understood from Eq. (16-19) which shows that the admittance area remains constant under a slow change in $B(z)$. The maximum size and maximum transverse momentum are $\xi_{\max} = \{2u/[e\pi B(z)]\}^{1/2}$ and $(p_\xi)_{\max} = [euB(z)/(2\pi)]^{1/2}$ from which it can be seen that, as $B(z)$ decreases, the size of the beam increases and the transverse momentum decreases. The interesting feature is that the transformation is independent of energy, so that the system is inherently broad-band in energy acceptance and can accept a large fraction of the initial positron spectrum.

The optimum conditions for the tapered solenoid are

admittance

$$U = \frac{\pi}{2} eB_f a^2 \quad (16-26)$$

initial field

$$B_i = \frac{a^2}{x_i^2} B_f = \frac{2}{\pi} \frac{U}{ex_i^2} \quad (16-30)$$

field profile

$$B(z) = \begin{cases} \frac{B_i}{1 + \alpha z} & z \leq L \\ B_f & z \geq L \end{cases} \quad (16-31)$$

length of tapered field

$$L = \frac{1}{\alpha} \frac{B_i - B_f}{B_f} \quad (16-32)$$

where

$$\alpha = \varepsilon \frac{eB_i}{m\Gamma} \quad (16-33)$$

and ε is an arbitrary small number of order 0.1; the other parameters have been defined earlier. The specified field profile results from the adiabatic validity condition, Eq. (16-16), with the assumption that the inequality should be equally well satisfied everywhere.* The useful energy bandwidth is limited at low energies by phase slip and at high energies either by phase slip, by failure of the adiabatic approximation, or by cutoff of the natural positron spectrum.

On the basis of the SLAC parameters, namely a design admittance of $U = 0.15\pi$ (MeV/c)(cm) and an accelerator aperture $a = 0.95$ cm, and assuming an effective source radius of $x_i = 0.2$ cm, one obtains $B_f = 1.1$ kG and $B_i = 25$ kG for the "optimum" final and initial fields. Actually a value of $B_f = 2.4$ kG has been chosen; this choice has the consequence that the useful positron beam in the uniform field region is confined to a radial size of $(x_f)_{\max} \approx 0.64$ cm which presumably makes the beam steering less critical in this region. On the other hand, the initial field is limited by practical considerations to a value of $B_i = 20.4$ kG, so that the initial matching is not quite optimum. The useful initial transverse momentum acceptance under these conditions is

$$(p_{xi})_{\max} \approx 0.7 \text{ MeV}/c$$

The field profile is based on an arbitrary choice of $L = 25$ in. for the tapered region, so that

$$B(z) = \frac{20.4 \text{ kG}}{1 + 0.118z(\text{cm})} \quad (16-34)$$

Taking the design energy to be $m\Gamma = 8$ MeV, one then finds that the adiabatic parameter, ε , is

$$\varepsilon = \alpha \frac{m\Gamma}{eB_i} = 0.154$$

The total Larmor angle through the tapered region is

$$\mu = \frac{1}{2} \int \frac{eB}{m\Gamma} dz = \frac{1}{2\varepsilon} \ln \frac{B_f}{B_i} = 2.2\pi \text{ rad}$$

* It is assumed that the taper takes place at constant positron energy, i.e., before entering the accelerating field.

There is an additional 5 in. of uniform field making a total of 30 in. between the radiator and the start of acceleration.

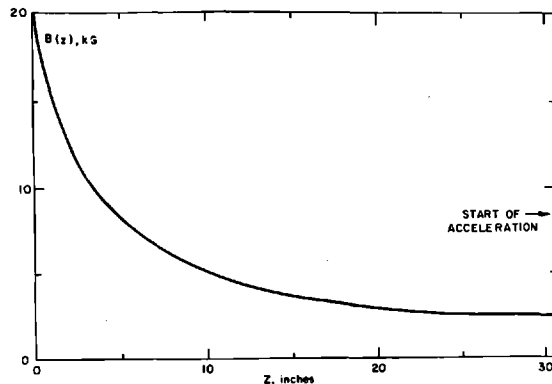
The useful energy acceptance is limited to a band from about 6 to about 11 MeV by velocity-dependent debunching, the first term of Eq. (16-25). The phase-angle spread in this band is about 14° , corresponding to a final spectrum width of $\approx 0.75\%$ for accelerated positrons. The maximum slip introduced by the phase-space-dependent effect, the second term in Eq. (16-25), is estimated as about 7° , which should not deteriorate the final spectrum seriously.

Figure 16-7 shows (a) the idealized field profile of the SLAC tapered solenoid and (b) the theoretical phase-space transformation from the source plane (admittance) into the uniform solenoid (emittance).

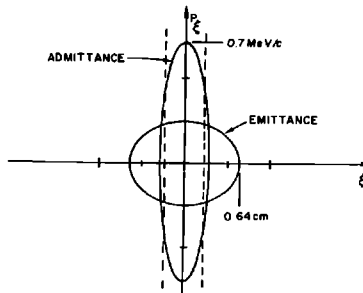
In summary, it is interesting to compare the properties of the quarter-wave transformer and the adiabatically tapered solenoids used as positron matching devices.

The quarter-wave transformer is characterized by rather moderate field strength requirements [note that $B_i = (a/x_i) B_f$], efficient use of magnetic field

Figure 16-7 Parameters of SLAC tapered positron solenoid.



(a) IDEALIZED FIELD PROFILE. THE FINAL VALUE OF 2.4 KG CONTINUES FOR APPROXIMATELY 25 FEET



(b) PHASE SPACE TRANSFORMATION

(e.g., relatively small stored energy), small RF debunching, and narrow-band acceptance of positron energies. These features tend to make this scheme ideal for machines in which the final positron energy is to be moderate or low, e.g., less than 1 GeV.

In the tapered solenoid, on the other hand, the field strength requirement tends to be rather extreme [note that $B_i = (a/x_i)^2 B_f$], and the magnetic energy is rather large (e.g., in the SLAC case, the power required for the 25-in. tapered field is comparable to that for the 25-ft uniform field section). The RF debunching tends to be severe, although the SLAC design is by no means optimized in this respect. The great advantage of the tapered system, for a very high energy machine, is its broad-band energy acceptance leading to theoretical positron yields of about an order of magnitude greater than for the quarter-wave transformer design.

Another advantage of the tapered system is that the field profile is quite uncritical. Because there is no need for a rapid transition from maximum to minimum field, the coil apertures may be quite large, thus providing space for protective collimators to shield the coils and accelerator structures from radiation. This feature is important in the SLAC case, where the power sprayed out of the radiator may be in excess of 100 kW; in fact, the need for the protective collimator is the main reason for placing the radiator 30 in. ahead of the first accelerator section, even though the debunching is worsened by this rather long drift length.

The validity of the adiabatic approximation has been probed by computer ray-tracing. It is found that the adiabatic approximation, with the field profile given above, is valid up to energies of about 30 MeV which corresponds to a value of ε of 0.58.

LONG-RANGE FOCUSING—QUADRUPOLES. In order to avoid the expense of extending the solenoids along the entire machine, a transition to quadrupole focusing is made as soon as the positron energy is high enough to permit reasonable spacing between the quadrupoles. For operational convenience, it was decided to use quadrupole multiplets—triplets or doublets. If the multiplets are short compared to their spacing, they may be treated to a first approximation as ideal, circularly symmetric, thin lenses.

The transport properties of such systems are summarized in some detail in Chapter 7. In the thin-lens approximation, the maximum phase ellipse which can be transported between two lenses located at z_n and z_{n+1} is

$$U_n = \frac{\pi a^2}{l_n} \quad (16-35)$$

where

$$l_n = \int_{z_n}^{z_{n+1}} \frac{dz}{P} = \frac{1}{m\gamma'} \ln \frac{\gamma_{n+1}}{\gamma_n} \quad (\text{assuming uniform acceleration}) \quad (16-36)$$

a is the limiting aperture, and $\gamma' = d\gamma/dz$.

Thus, to maintain a given admittance U through the system, the optimum lens spacing is

$$\begin{aligned} L_n &= z_{n+1} - z_n = \frac{\gamma_n}{\gamma'} (e^\beta - 1) \\ &= L_0 e^{n\beta} \end{aligned} \quad (16-37)$$

where

$$\beta = \frac{\pi a^2 m \gamma'}{U} \quad (16-38)$$

and

$$L_0 = \frac{\gamma_0}{\gamma'} (e^\beta - 1) \quad (16-39)$$

The focal lengths of the lenses are, then,

$$F_n = \frac{1}{2} \gamma_n l_n = \frac{\pi a^2 \gamma_0}{2U} e^{n\beta} \quad (16-40)$$

With the SLAC design parameters, $a = 0.85$ cm, $U = 0.15\pi$ (MeV/c)(cm), $m\gamma' \approx 0.06$ MeV/cm, and an arbitrary assumption of $L_0 = 300$ cm for one accelerator section, one obtains $m\gamma_0 \approx 53$ MeV for the positron energy at which the quadrupole focusing can begin. About twelve lenses would be required to taper up to a spacing of one sector $\approx 10^4$ cm, to match into the regular sector doublet focusing system.

The actual SLAC system uses compact, small aperture quadrupoles (0.6-in. bore radius, 4 and 8 in. in effective length). The overall physical length of the special multiplets is about 28 in. To make space for these multiplets, special, short (7 ft long) accelerator sections were fabricated. This system avoids the necessity of large aperture quadrupoles to fit around the accelerator sections (≈ 3 -in. radius) but makes it impossible to place the lenses with precisely the theoretical optimum spacing given above. Rather, the theoretical spacings were used as a guide in selecting the maximum allowable spacing between any pairs of lenses.

Figure 16-2 shows the locations of the various special focusing elements. Here S-1, S-2, . . . , S-13 are the special short multiplets and D11, D12, etc. are the regular sector doublets. Note that the regular doublets D11 through D14 are used as elements in this focusing system. In the original design concept, all of the multiplets were triplets. However, as part of the beam breakup improvement program,* all the sector lenses and some of the special positron lenses were converted to doublets. As of the present time (July 1967), lenses S-1 through S-6 are triplets and the remainder are doublets.

The TRANSPORT computer program has been used to determine the correct quadrupole settings. Figure 16-8 shows the theoretical admittance plots obtained by mapping the various defining apertures to the output end of the uniform field solenoid.

* See "The Magnetic Fix Program" in Section 7-5.

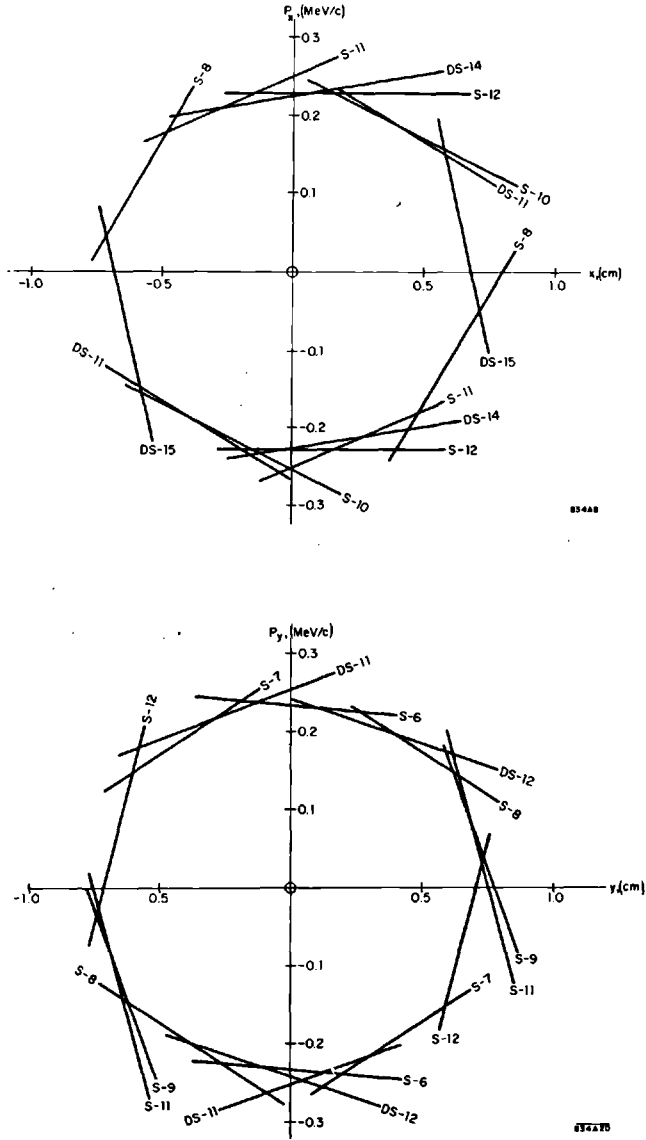


Figure 16-8 Computed admittance of long-range positron transport system, referred to the output end of the uniform solenoid; quadrupole strengths approximately optimized. Only those apertures that actually affect the admittance have been mapped on these plots (see Figure 16-2 for lens designations). (a) x, p_x plane; admittance $\cong 0.163\pi$ (MeV/c)(cm); (b) y, p_y plane; admittance $\cong 0.166\pi$ (MeV/c)(cm).

16-3 Radiators (CTH)

Three different radiators are described in this section: the “slug” (temporary source), the “wand” (a few pulses per second source) and the “wheel” (continuous source). An overall view of the positron radiator area is shown in Fig. 16-18.

Before the construction of the wheel radiator could be completed, a continuous source of positrons was needed that could accept higher-power levels than the wand target is capable of handling when held stationary in the beam. This was the function of the slug.

Slug radiator

The slug radiator is a water-cooled copper block that can be held in the beam or retracted to allow operation of the wand.

TARGET. The target is a cylindrical block of OFHC copper (see Fig. 16-9) which has been slotted radially to provide water channels in a spiral configuration, but to a depth that keeps solid copper throughout the beam path. The block is brazed into a stainless steel case that forms the water chamber. The copper block is exposed only at the entrance and exit of the beam. Cooling water from a manifold (visible in Fig. 16-10) is injected at three points around the stainless steel case and flows axially through the slots to output tubes leading to a second manifold.

RETRACTION. A commercial pneumatic cylinder slides the support rod through pillow blocks for insertion and retraction. A bellows seals the vacuum chamber. To hold the vacuum load when air is turned off, a mechanical latch engages the support rod in the retracted position. The latch is lifted by a solenoid.

The control valve for the actuator is solenoid-operated and is mounted on the actuator stand. Flow control valves (needle and ball check) between the control valve and the actuator prevent rapid motion of the target.

SENSORS. Limit switches are tripped at each limit of travel. Signals appear on the instrumentation and control panel indicating “slug in,” “slug out,” and “in transit,” and interlocks with the wand and with the beam are activated.

The exit face of the copper block carries three thermocouples that monitor the steady-state temperature at the edge of the beam and also indicate centering of the beam.

FLANGE. The flange for the slug radiator is the same as that for the wheel radiator described below.

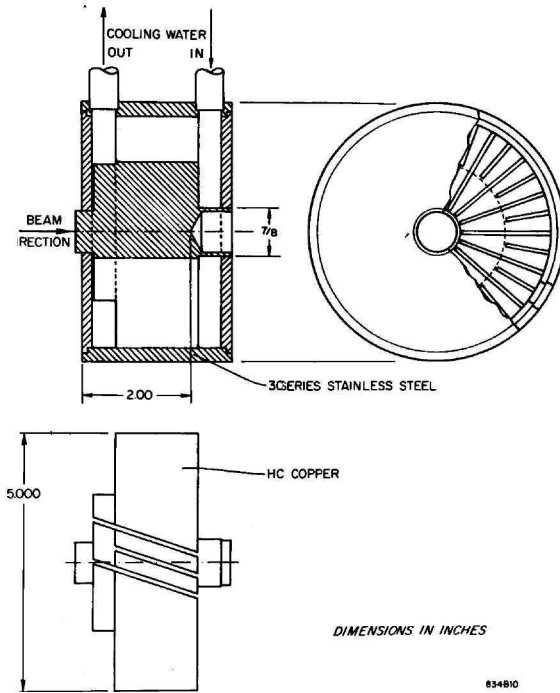


Figure 16-9 Assembly of slug radiator.

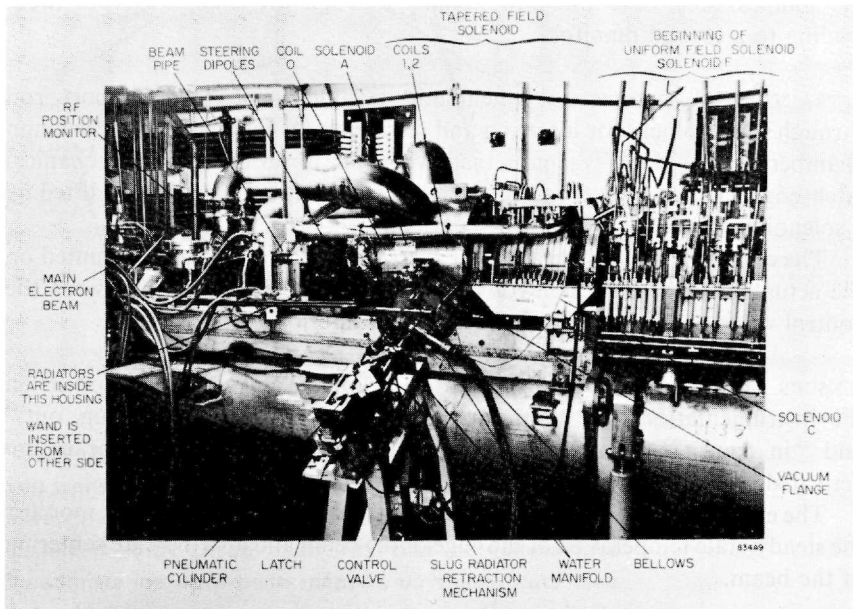


Figure 16-10 Overall view of positron radiator area with slug radiator installed.

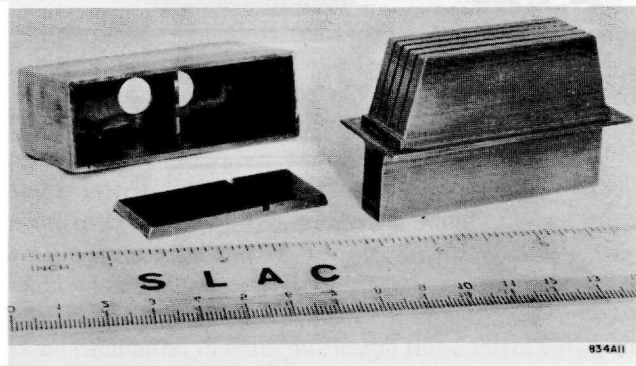
Wand radiator

The wand radiator converts a particular electron beam pulse to positrons while allowing free passage to the other electron pulses. In operation, a slim arm swings the target through the beam. The speed of passage could not be too high because of the difficulty of synchronizing the center of the swing to the electron pulse timing. In actual operation, nine consecutive electron pulses (at the 360-pulses/sec repetition rate) are interrupted by inhibiting the trigger to the injector. This inhibition is lifted for the fifth pulse which produces the positrons. Positrons can also be produced on the return swing, and up to several positron pulses per second are possible. For some operating conditions, more than nine electron pulses must be interrupted because eddy currents in the radiator steer the electron beam which is only a fraction of an inch away.

TARGET. The target which is inserted into the beam consists of a solid copper block, 2.25 in. long in the beam direction (see Fig. 16-11). It is 0.38 in. wide in the direction of its swing and maintains this width over a height such that even a poorly centered beam is intercepted. Then it widens to 0.75 in., the width of five fins with 0.03-in. cooling-water slots. A stainless steel baffle plate covers the top edge of the slots to force the water to run along the full length.

A rectangular cover, also of stainless steel, is brazed to a shoulder around the copper block. The cover is the structural attachment for the target and also confines and directs the cooling water. After brazing the cover to the copper block, the end of the copper where the beam leaves the target is cut away about 0.26 in. to give the desired length of 2.25 in. Because showering increases through the block, the exit face has maximum heating; the removal of part of the copper has the effect of increasing the available cooling where it is most needed.

Figure 16-11 Wand target with stainless steel baffle plate and cover.

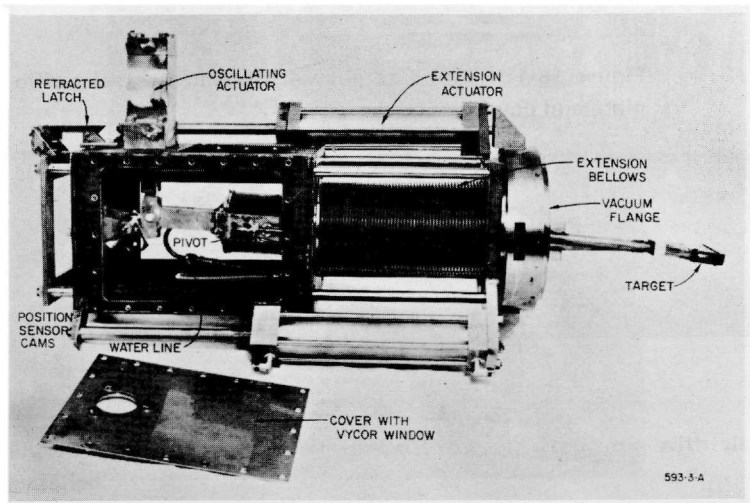


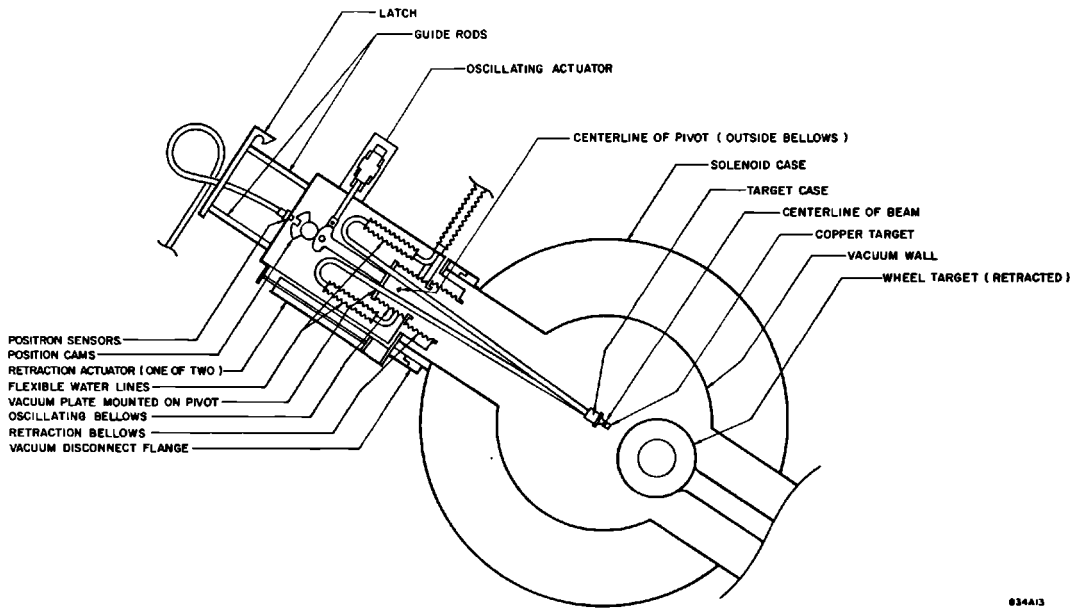
An alternative target, consisting of eleven plates normal to the beam with cooling water flowing between them, was built and tested. It had the disadvantage of requiring thin windows to separate water and vacuum along the beam line and its output of positrons gave only two-thirds of the production obtained from solid copper. This alternative target is shown in Fig. 16-12, attached to the wand actuation mechanism.

WAND. The wand itself is a pivoted support arm for the target case. It consists of two water tubes of 321 stainless steel (see Fig. 16-13) which are welded through the vacuum plate and end in flexible metal hoses. The vacuum plate is supported by two rocking brackets from the pivot. A drive arm connects the vacuum plate to an adjustment link on the oscillating actuator. Vacuum integrity is maintained by an oscillating bellows that seals the vacuum plate to the floor of the box. The pivot bearings straddle this bellows so that its midpoint lies on the pivot center line. When the wand oscillates, the bellows follow a simple rocking motion with stresses low enough to assure long life. Because of the rocking motion, journal bearings were used for the pivot. In order to withstand radiation, the bearings were turned from sintered bronze and vacuum impregnated with Shell VRT fluid E.

OSCILLATING ACTUATOR. The oscillating actuator consists of a pneumatic piston and cylinder, with air cushions at each end operating through the entire stroke. The cushion plungers are integral with the piston and nearly as large in diameter. The piston and plungers, as well as the piston rod seal, are made

Figure 16-12 Wand radiator and actuation mechanism ready for installation in the accelerator (target shown, requiring thin windows, was later replaced by the target shown in Figure 16-11).





034A13

Figure 16-13 Diagram of wand target, positron source.

of impregnated bronze. Air leakage is controlled by close fits to the stainless case. Ball and needle valves in each end of the case control the cushioning. An adjustable link connecting the piston rod to the drive arms allows the wand to be roughly centered. Exact centering is not needed; it is necessary to know only when the wand passes through the beam and this is accomplished by adjustment of the position cams. An air valve, selected for fast response, controls the air to the oscillating actuator. The two solenoids that drive the valve spool are rated for ac power but are energized by a dc pulse to avoid time lags due to phasing. This valve must be connected by short lines to the actuator and is, therefore, mounted on the side of the positron strongback in the tunnel.

FLANGE. The wand flange carries a shallow, polished groove while the mating flange on the solenoid case has a deep, polished groove. The grooves were designed for a commercial seal ring but a solid indium ring of square cross section has proven superior.

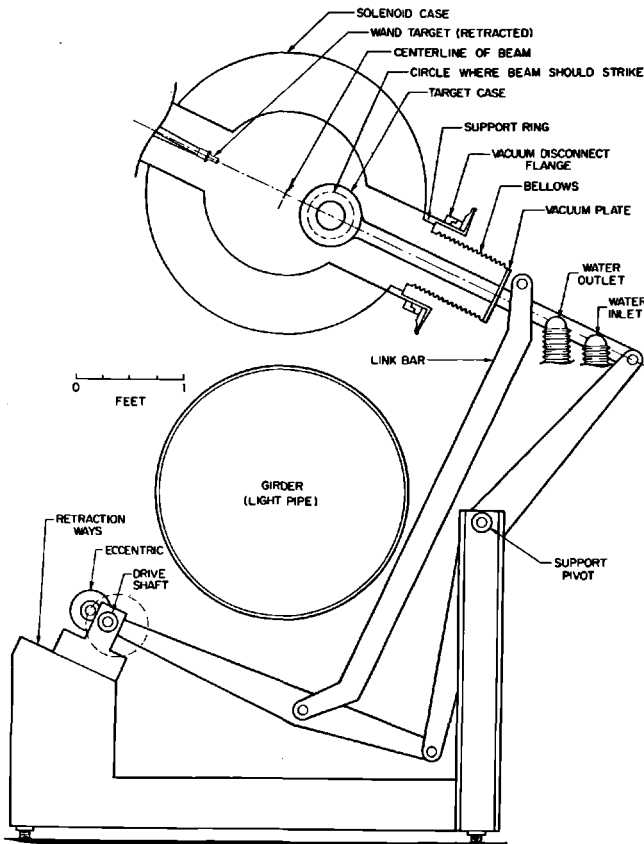
OPERATION. The wand is interlocked to prevent insertion if the wheel target is occupying the chamber, to prevent oscillation if either wand or wheel microswitches change to an "in transit" signal, or if the vacuum, air, or water fail. The beam is interlocked while the target is close to the beam center line. Air to the oscillating valve in the tunnel passes through a control valve in the gallery. All interlocks on oscillation operate by closing this control valve. The

speed of the wand travel may be varied somewhat by altering the air pressure into the control valve by means of the regulator on the air panel in the gallery. Large changes in pressure require resetting of the cushion needle valves in the oscillating actuator to prevent impact or bounce. The latch and the centering bellows are actuated by air from the same regulator but their functions are independent of the air pressure within wide limits.

The wand moves across the beam line at a speed of 50 cm/sec, and it may be driven across up to 3 or 4 times/sec.

A small, spring-return bellows is mounted on the lower side of the wand box. The moving end of the bellows is connected by a small cable to the driving arm inside the box. When this bellows is actuated, the cable is pulled down to a stop and holds the wand target in the beam center line. This "hold" is used if the wand is to function as a fixed target. The flexibility of the actuating cable prevents the "hold" system from interfering with the normal oscillating motion of the wand.

Figure 16-14 Diagram of wheel target, positron source.



Wheel radiator

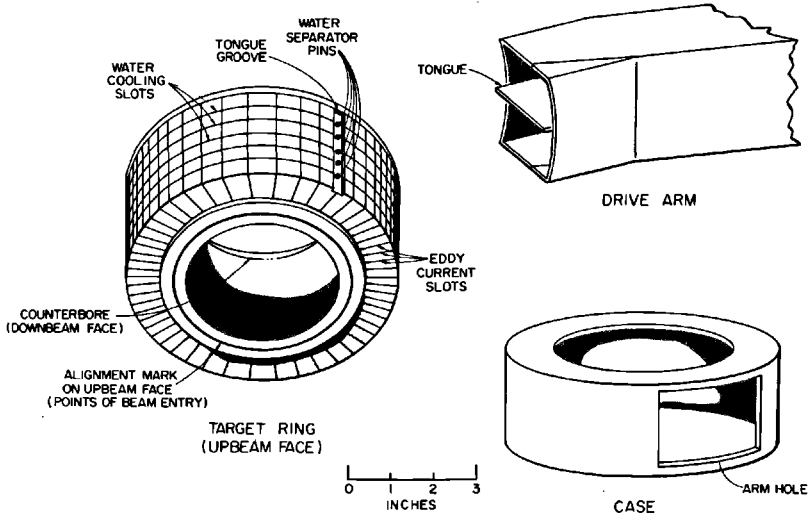
The wheel radiator is designed to provide positrons up to a repetition rate of 360 pulses/sec, using full electron beam power at Sector 11. The target moves in a circle with sufficient speed to minimize the overlap by successive incident beam pulses. Because of concomitant sealing problems, the driving mechanism was designed not to rotate but to "troll" the target (see Fig. 16-14.)

TARGET. The target is a solid copper ring, 2.1 in. thick along the beam axis with circumferential water-cooled fins. A stainless-steel case covering the fins contains the cooling water and is welded to the drive arm (see Fig. 16-15). The case is brazed to the copper at a radius sufficient to prevent the beam from hitting the joint under any condition of steering.

A series of pins blocks the water slots at the junction with the drive arm to prevent short-circuiting between inlet and outlet water flows. Because of the increased particle flux from showering, heat deposition increases through the ring. The downbeam face of the ring has, therefore, been counterbored so that, in effect, two additional fins cool the hotter section. The design assumes a 50-kW thermal deposition in the last third of the ring and a total of 100 kW in the entire ring.

The peak temperature of the copper depends, of course, on the thermal path length to the nucleate boiling level. For this reason, the solid ring is only 0.375 in. wide radially, and the center line of the beam pipe is just 0.150 in. from the edge of the central hole in the target ring. If the beam is misdirected,

Figure 16-15 Details of wheel target, positron source.



on half of the trolling cycle it will hit closer to the cooling fins, and on the other half, it will miss the target entirely.

In a continuous copper ring trolling in a magnetic field, eddy current drag could be substantial. A series of radial slots at right angles to the cooling fins are made to reduce these currents.

TROLLING DRIVE. Several methods for generating circular motion without rotation were studied. A true pantograph linkage could have provided perfectly circular motion, but either large forces or interference with the overall structure would have resulted. A modified pantograph was chosen (Fig. 16-14) in which the offsets of the support pivot and the link pivots reduce the target deviation from a circle to 0.072 in.

A three-phase induction motor drives a worm reducer (15:1) through an electric clutch-brake. A pair of replaceable gears transfers the 116-rpm output of the worm to the drive shaft of the eccentric. For the present target, which requires a 5.25-in. diameter trolling circle, the transfer gears have a 1:1 ratio. For other targets or a wider beam spot spacing, the transfer gears can be replaced for stepped speed changes.

RETRACTION. The transfer gears are connected to the drive shaft of the eccentric by means of two universals and a spline. Since the eccentric bearings are mounted on ways, the shaft arrangement permits the eccentric mounting to be shifted 3.25 in. (up to the left in Fig. 16-14) without disturbing the gears or motor. Through the linkage, this movement retracts the wheel target from the beam center line to permit the passage of electrons or to leave room for the wand target. Travel is controlled by limit switches which also actuate interlocks on wand insertion or beam pulses and which light three indicators in the instrumentation and control alcove: "wheel in," "wheel out," and "in transit." The motor has a spring brake that releases when power is turned on.

SENSORS. In order to retract the wheel, it must stop trolling in the zero position in which it is shown in Fig. 16-14. To accomplish this, a ferrite "proximity sensor" follows a cam on the downbeam extension of the drive shaft. The cam edge is a solid circle except for one notch which generates a square pulse in the sensor at the zero position on each revolution. Upon the retract command, a delay is activated which starts timing at the next sensor pulse. At the end of the adjustable delay interval, the drive clutch is opened and the brake applied. The linkage stops in the zero position with the proximity sensor signaling the presence of the notch. This signal releases an interlock and starts the retraction motor.

Two pulses in the same spot on the target ring would increase the chance of thermal fatigue; more than two pulses would be needed to distort or melt the copper. In the event of clutch slippage or motor overload, the most likely causes for loss of speed, the beam must be interrupted. A small gear acts as a second cam and is mounted next to the first. A timing circuit checks the period

between teeth passing under a second proximity sensor and interrupts the beam if the period lengthens. If the transfer gears are changed to run at a different speed, the speed cam is changed to match it.

FLANGE. The vacuum disconnect flange is similar to flanges used in the BSY with minor modifications. Two hooks on eccentrics clamp the flanges together by means of two ring springs. These rings have been machined with six equally spaced lands that contact the flange lip at different level of clamp pressure. Fully clamped, the rings distribute equal forces to the flanges at each land. The two-point actuation allows the flanges to be opened easily from a distance.

The seal is a ring of solid indium of rectangular cross section. It is trapped in a groove and forced to extrude slightly.

To prevent the varying spring forces generated by the bellows from disturbing the indium seal, a support ring is attached to the solenoid case inside the flange to provide a rest for the bellows terminal. The connection between the flange and the bellows terminal is welded from flat, light, stainless sheet, so that the flange is effectively isolated from the bellows forces transmitted through the support ring.

OPERATION. To run the wheel target, a switch on the instrumentation and control panel is turned. If the wand cooling-water and vacuum interlocks are clear, the retraction motor inserts the wheel to the zero position. The limit switch both stops the retraction motor (and switches its line connections to reverse) and actuates the trolling clutch. The last interlock clears when the speed sensor indicates trolling speed.

If the wand slips from the retracted position or if the vacuum interlock is activated, wheel rotation stops automatically. Other interlocks interrupt the beam. To retract the wheel manually, the panel switch is again turned and the trolling stops with the wheel in the zero position. The retraction limit switch stops the motor, reverses it, and clears the interlocks.

FLOOD CONTROL. The large water capacities, separated from the accelerator vacuum by stressed metal and brazed or welded joints, pose a hazard. The working bellows are an additional hazard but because they separate air from vacuum, the consequences of a failure are less severe. To limit damage, the first 10-ft positron girder has a separate vacuum system with its own ion pump. The accelerator vacuum header skips this girder. A fast valve at each end of the girder isolates the positron section from the accelerator sections on either side. In addition to these passive design features, an active system responds automatically to pressure increases in the positron chamber.

An ion gage monitors the vacuum line a few feet from the positron chamber. If the pressure rises to 10^{-5} torr, the beam is interrupted. An increase to 5×10^{-5} torr is assumed to be a small leak; the fast valves close to isolate the section, and solenoid valves cut off the water supply to both wheel and wand.

If the wand is in use, the oscillating air is vented and the wand settles by gravity to the lower end of its swing. If the wheel is in use, it stops trolling and retracts out of the beam line.

If the pressure continues to rise to 10^{-2} torr, dry nitrogen is released into the chamber and allowed to build up to 5 psig. At this point, drains open at the lowest point in the water lines, so that flow through either an air or water leak is reversed.

16-4 Design and construction of the solenoids (HB and KGC)

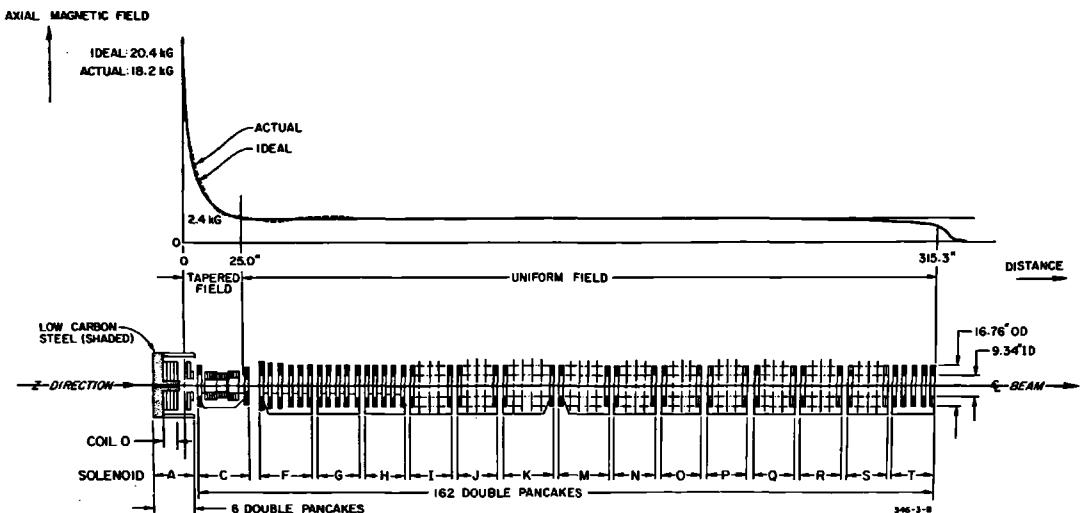
The principle of the tapered-field solenoid has been described earlier in this chapter. It was decided to build a solenoid that generates a longitudinal field along the beam axis as shown in Fig. 16-16. If $z = 0$ is taken at the target face of the positron radiator, the desired field for positron focusing at any point z (in centimeters) downbeam has been shown to be given by the expression

$$B_z = \frac{20.4}{1 + 0.118z} \text{ kG} \quad (16-34)$$

Thus, the 20.4-kG longitudinal field at $z = 0$ must be tapered to 2.4 kG at $z = 63.5$ cm. A uniform field with an amplitude for 2.4 kG should be maintained for another 7 meters downbeam.

To help fulfill these requirements, an additional magnet (coil 0 in Fig. 16-16) with a central field of 37 kG, generating 12 kG at $z = 0$, was added upbeam from the radiator chamber. Superposition of fields originated by coil

Figure 16-16 SLAC positron solenoid.



0, iron, and downbeam coils, yields a total field at $z = 0$ of 18.2 kG, which corresponds to 89% of the specified field value.

Much of the difference between the ideal and calculated field at $z = 0$ is due to limitations on the size and location of coil 0. The outside diameter of coil 0 was severely restricted to avoid blocking two lines of sight for optical tooling. These lines extend uninterrupted over the full length of the accelerator, 25.4 cm below and 13.7 cm on each side of the beam axis. The location of the center of the coil at $z = -16.71$ cm was dictated primarily by mechanical and heat transfer considerations. To force the maximum field downbeam, an iron return path (see Fig. 16-16) was provided along the inside diameter and the upbeam face of the coil. The measured field contribution from coil 0 and iron at $z = 0$ is 13.7 kG, i.e., approximately 1 kG less than calculated. The discrepancy is believed to be primarily due to the poor magnetic quality of commercially available low-carbon (1010) steel, used without previous annealing.

By balancing the magnetic requirements with those for mechanical support of the disk-loaded waveguides and associated cooling water, vacuum and RF connections, a constant 9.91-cm center-to-center spacing was maintained between matched pairs of double coil "pancakes" throughout the uniform field. The dip in the field curve between double pancake pairs was on the order of 4 G. For ease in manufacturing, 142 of the 146 hollow conductor double pancakes in the uniform field had identical dimensions. The other four differed only in outside diameter.

The double pancakes adjacent to the positron radiator are subjected to a relatively high integrated radiation dose. Since it was difficult to make correct estimates of the maximum dose rate, the insulation which was chosen was of the type developed at SLAC for maximum radiation resistance, using glass tape impregnated with alumina-loaded epoxy.¹²

Because of the high-power density and heat flux, 32.5 W/cm³ and 121 W/cm² (maximum), respectively, edge-cooling was required in coil 0. Chromium plating was applied over a nickel substrate to protect coil surfaces exposed to erosion by water with a velocity as high as 6.5 meter/sec.

Figures 16-10 and 16-17 through 16-19 show the solenoids installed in the positron source station in Sector 11. Solenoids A and C are identified in Fig. 16-10. Although unidentified, solenoid F appears just to the right (downbeam) of solenoid C. Access to the radiator chamber is through the flanged opening in the side of the solenoid A housing. Labels indicate the relative position of edge-cooled coils 0, 1, and 2 within the housing.

Figure 16-17 includes the full complement of uniform-field solenoids. In this view, the upbeam cover and all but one of the double pancakes of coil 0 have been removed from solenoid A, exposing the four feedthroughs and the shaft upon which the double pancakes are centered.

Figures 16-10 and 16-18, looking at the same general area, illustrate the complex array of power, water, and other utility connections required to service a solenoid installation of this magnitude. Figure 16-19 was taken looking upbeam at the downbeam end of the positron source station.

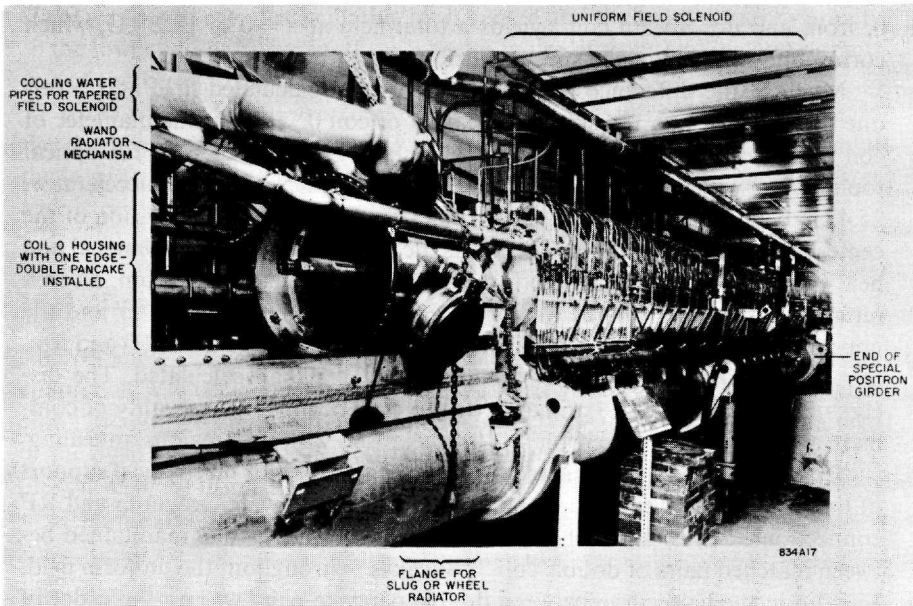


Figure 16-17 General view of positron radiator area. Coil 0 housing open, wand radiator installed; wheel or slug radiator not installed.

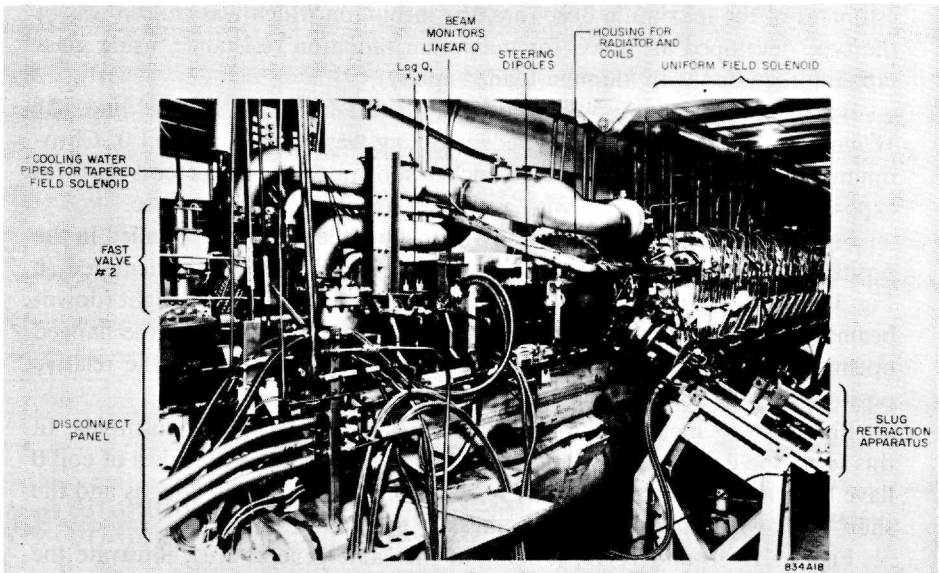


Figure 16-18 General view of positron radiator area. Slug radiator installed; wand radiator not installed.

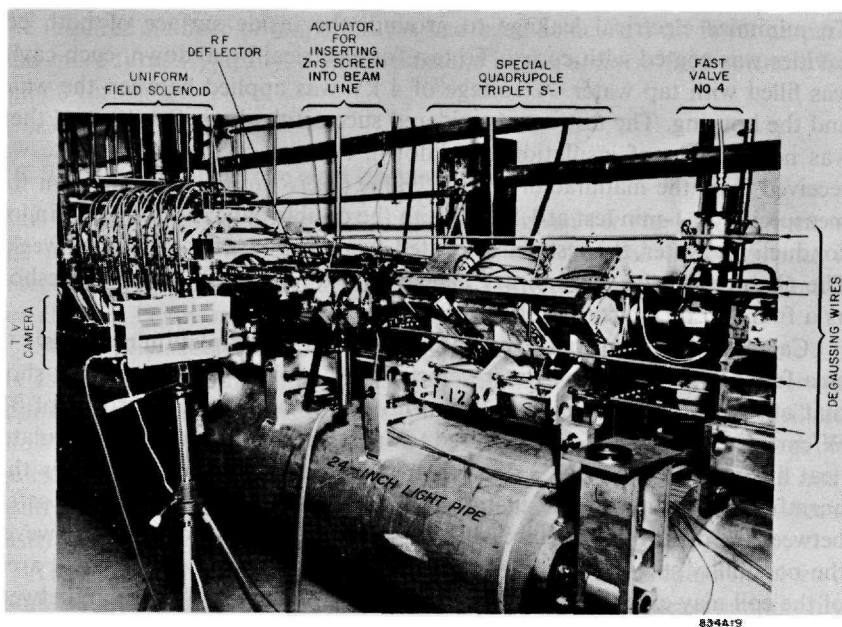


Figure 16-19 General view of downstream end of special positron girder. Beam direction left to right.

Coil design

Double pancake design for a succession of coils producing a specified longitudinal field is generally governed by Fabry geometry factors.¹³ Since mechanical obstacles prevented full optimization, trial and error calculations performed on the computer were used to give the best results to obtain a satisfactory field distribution.

No major problems were encountered in cooling the seventy-eight hollow conductor coils in the uniform-field solenoid and in frame C of the tapered-field solenoid. Values of heat flux, an order of magnitude higher than in the hollow conductor wires, required that considerably more attention be given to the cooling of coils 0, 1, and 2. To improve mechanical strength between double pancakes and reduce the danger of electrical breakdown due to creeping along immersed surfaces, water cooling was confined to the conductor edges on the two outside faces of each double pancake. As finish-machined, the conductor is 0.635×1.59 cm in cross section and slightly tapered toward the ends to leave more room for insulation between the edge exposed to water flow. The glass tape and cloth used as insulation was prefilled with alumina-loaded epoxy. After winding and vacuum impregnation, double pancake faces were carefully machined. To insure that all surface cracks and minute voids exposed by machining were filled, each double pancake was then reimpregnated.

Coil 0 is a stack of four edge-cooled double pancakes, three dividers, and two end spacers mounted in the upbeam coil cavity of the solenoid A housing.

To minimize electrical leakage to ground, the inside surface of both coil cavities was coated with epoxy. To test for electrical breakdown, each cavity was filled with tap water. A voltage of 4 kV was applied between the water and the housing. The test was considered successful when after 10 min, there was no evidence of insulation breakdown. After each double pancake was received from the manufacturer, its Q value ($\omega L/R$) in the dry condition was measured by a 1-min test at 1.5 kV. With the double pancake immersed in low conductivity water, the test was repeated every 24 hours for the next 2 weeks. The Q values of the wet and dry pancake were compared. Corona threshold as a function of interturn voltage was also recorded.

Calculations of burnout temperatures by various correlation methods¹⁴⁻¹⁷ as a function of heat flux, water velocity, and coolant slot dimensions show that at the design water-flow rate, burnout may occur at a heat flux of 371 W/cm². Comparison of the measured temperature gradient and the calculated heat flux indicates (1) a heat flux under operating conditions well below that harmful to the interturn insulation and (2) a considerable margin of safety between the operating heat flux and the corresponding burnout flux. However, the possibility still exists that the operating heat flux in certain critical areas of the coil may exceed 121 W/cm², thereby justifying a 300% margin between calculated values of heat flux and burnout heat flux.

The shape of the measured magnetic field agrees well with the calculated field; the absolute values agree within about 5% which is comparable with the uncertainties in the calibrations of the measuring equipment.

The power supplies for the solenoids have silicon controlled rectifiers and are current regulated to about 1% at full power. Since the energy acceptance of the focusing system is broad, good regulation is not required. One supply powers coil 0 to 700 kW (3720 A, 188 V); another powers coils 1 and 2 and frame C, the remainder of the tapered-field solenoid, to 116 kW (2000 A, 58 V); and a third one powers the uniform-field solenoid to 253 kW (two solenoids in parallel, each at 600 A, 211 V).

Because the positron beam has a rather low energy while it is in the solenoids, it was desirable to minimize stray, transverse magnetic fields which could mis-steer the beam. Therefore attention was given to the cancellation of stray fields from the leads and to the alignment of the various magnetic elements that give rise to the longitudinal field. Typically, the tolerance on the angular alignment of the axis of a magnetic element was 2 mrad.

The uniform field solenoid was divided into fourteen separate frames, each of which contained five or six pairs of double pancakes. Within a frame, the double pancakes were aligned to minimize the transverse field, and the alignment of each frame on the strongback was checked by verifying that the net steering effect was small. Asymmetries arising from the leads, crossovers within double pancakes, and cross-connects between double pancakes were cancelled to a large extent because the solenoid was actually made of two interlaced solenoids, each with opposite helical pitch. The problems associated with alignment and stray field effects would probably have been less severe if

the required number of ampere-turns had been achieved with fewer amperes and more turns (typically, a single pancake in the uniform-field solenoid has only 8 turns).

16-5 Instrumentation and control (KEB)

This section discusses some of the guidelines given for the development of the positron beam instrumentation and control and the problems met in integrating the necessary signals and controls with the existing instrumentation for electron beam operation from the CCR.

Sector 11 was selected for the location of the positron source with most of its associated equipment. The beam monitoring and steering system in the following four sectors was to be augmented by special devices to facilitate the monitoring and guidance of the established positron beam. The need for quick access to the special equipment made it desirable to locate the main control point in Sector 11. This location also made it possible to set up special instrumentation quickly.

The overall operational concept assigned to CCR all functions involved in establishing and controlling the electron beam. However, at least temporarily, when the positron beam is being generated, all subsequent operations are to be directed from Sector 11, with CCR assistance only when requested. Later on, it is anticipated that positron operation will be feasible from CCR when all special routines have been established. For this reason, all local instrumentation for positron operation in Sector 11 had to be made compatible for remote control.

Instrumentation requirements

The positron control and instrumentation requirements called for individual RF power control and monitoring of the two klystrons following the positron source. Suitable controls, monitoring, and protection were required for the "wheel" and the "wand." Current control and monitoring for each of the three power supplies servicing the focusing solenoids were also specified.

In addition, instrumentation was required for the thirteen special quadrupole packages following the solenoids. Eight of these are located in Sector 11, three in Sector 12, and one each in Sectors 13 and 14. Access to the standard beam guidance and monitoring equipment in Sectors 11 through 14 is required. The phasing system in Sector 11 had to be modified to permit both local, individual, and remote automatic operation.

The positron control system resulting from the above requirements was installed in the instrumentation and control (I & C) alcove of Sector 11. The alcove is the data collection point in every sector and is, thus, the local interface between the accelerator and CCR. This location permitted easy access to the new equipment and interconnections with existing systems and CCR. Some of the major control features provided are described below.

Klystron voltage control and phasing

Two separate power supplies were installed to supply the operating voltage for the two klystrons following the positron source. The on-off and voltage control were of the same basic design as used in the control of the standard substations. The combination of standard reference voltage power supply and monitor rectifier could, therefore, be used to set the klystron voltage and to provide the “deQ’ing” level for the associated modulators. Two identical sets were installed.

A special panel was built for the power supply on-off control, which also displays the power supply and operating status of the special klystrons. These controls are presently operated from Sector 11 only. The contactors of the power supplies are interlocked with the personnel protection system and can be energized only when all interlocks to the accelerator housing are closed. The operating status of the special klystrons also controls the red-green warning lights in Sector 11.

All klystrons in Sector 11 can be phased from CCR in the usual manner. Local phasing of the klystrons is possible from a special local phasing panel; additional controls permit the “accelerate-standby” selection of individual klystrons.

Wand control

The essential operational and monitoring features for the wand control are located on one panel. It controls and monitors the movement of the wand from the retracted position, where it is normally held when not in use, into the operating position and vice versa.

When the wand has been moved “in,” another control permits it to operate in an oscillatory mode or in a stationary position in the beam line. The control selecting the oscillatory mode functions only when the wand is “in,” and operates into the wand driver unit which generates the drive pulses for the solenoids in the air system. An air-operated system, described earlier, is used to move the wand across the beam and to return it to its starting position.

Wheel controls

The wheel controls and monitoring signals are assembled on one panel. Ancillary equipment needed for the operation of the wheel and to monitor its movements is located in a special rack near the “penetration” to the wheel.

Similarly to the wand, the wheel is in a retracted position when not in use and is moved into an operating position where it can “troll” when a positron beam is to be generated. Two electrical motors are provided, one for the “in-out” motion and the other for the trolling motion. The motor for the trolling motion is coupled to the wheel through an electrically operated clutch-brake device.

The following operations take place when the control switch is placed into the "wheel in" command position. The motor assigned to this function is energized and moves the wheel in. When it is completely in, the motor is stopped and the trolley motor is started. Simultaneously, the brake is released and the clutch is engaged. The trolley motion starts, its speed is monitored and when a preset value is exceeded, an interlock is closed which in conjunction with other wheel interlocks permits the beam to be turned on. This sequence of operation is completely automatic, except for the beam turn-in. The individual stages are monitored and indicated on the control panel.

Solenoid power supply controls

Three power supplies for the operation of the tapered- and uniform-field solenoids were specified and procured from an outside vendor, who also furnished the control panel for the supplies. It provides for on-off and voltage control for each supply.

The solenoids have a very large number of interlocks which monitor the flow and temperature of the cooling water in individual coils. To facilitate fault location, these interlocks are monitored individually on a hold basis; i.e., when a fault has been cleared, the fault indication does not disappear until a reset button is actuated, which closes the interlock chain and permits resumption of operation.

Additional monitoring is done on a special panel summarizing the operating relations between the pump supplying cooling water to the solenoids and their power supplies.

Steering and quadrupole power supply controls

The above title is the name of a panel for beam guidance control. It was desired to control six steering dipoles and eighteen quadrupoles between Sectors 10 to 14. Because of the large number of access points, one set of instrumentation for quadrupole and steering current control was mounted on a panel with selector switches permitting the selection of the control point chosen. Four of these points were part of the standard beam guidance system controlled from CCR. Special relays were added in these locations to disconnect the CCR control temporarily while adjustments were made from the positron control point in Sector 11.

Beam monitoring

The standard beam monitoring system generates one signal proportional to the charge of the beam pulse (linear Q) and another signal indicating in sequence the logarithm of the charge and the horizontal (x) and vertical (y) positions of the pulse (see Chapter 15). These signals are normally transmitted to CCR and displayed with the signals from other sectors in such a way as to show the sector-to-sector variations of each quantity.

One set of FM receiving equipment for linear Q is installed locally in Sector 11, and a selector switch is provided on a special panel to connect the receiver to the location to be monitored. The output can be displayed on a scope.

Similarly, the composite signal ($\log Q, x, y$) is made available at Sector 11 for scope display by connecting the appropriate receiving equipment to the point chosen. A separate selector switch is provided on this panel.

The linear Q amplifier in each sector is adjustable in gain to cover the full range of the beam current. It also has a provision for reversing the input when a positron beam is to be monitored. The appropriate controls are also furnished on this panel.

Supplementary beam monitoring is provided by ionization chambers, sensitive toroid beam monitors, and fluorescent screens that can be inserted into the beam path at the special quadrupole multiplers. The screens are viewed with TV cameras (see Fig. 16-19). Several such cameras can be preset. The insertion and retraction of these special monitors is controlled from Sector 11. When a monitor is inserted, the copper walls of its vacuum enclosure cause so much scattering that the beam is no longer transmitted.

Radio-frequency deflection system

Under typical operating conditions, both positrons and electrons would be captured and accelerated at the same time, with the bunches of opposite sign riding one-half wavelength apart in the machine. The standard position and intensity monitoring devices cannot respond separately to these two beams, and special devices that could do so seemed complicated to build. A relatively simple solution was to utilize the RF structure of the beams and to deflect the unwanted particle bunches out of the machine.

One part of the deflection system is a traveling wave structure that gives the same horizontal impulse of about $0.5 \text{ MeV}/c$ to the bunches of both signs. The other part is a standard sector steering dipole adjacent to the deflector, which is pulsed to cancel the impulse on the desired bunches and to double the impulse on the unwanted bunches. These are, then, deflected into the walls of the machine, about 10 ft farther downstream.

The deflection occurs after about 70 MeV of acceleration, when the two beams are well formed. The RF deflector is about 24 in. long and operates in the HEM_{11} mode at 2856 MHz.¹⁸ Its power (typically about 1.5 MW peak) comes from the same klystron that powers the second 10-ft section of disk-loaded waveguide downbeam of the radiator. Since the magnet is triggered on a pulse-to-pulse basis, either a positron beam or an electron beam can be accelerated while the radiator remains fixed in the "in" position.

Central Control Room Signals

A minimum number of signals is presently transmitted to CCR until such time when positron operation can be performed from this point. The basic

concept for selecting signals considers two cases. For positron operation, CCR is to stay in close contact with Sector 11 and to be kept informed about the status of the operation. When positron beam operation is discontinued, CCR is to have sufficient information that equipment used for generating and monitoring the positron beam is shut off and, therefore, cannot interfere with the electron beam.

Supplementary status information is given about systems that either have to be kept in operation or are needed both for electron and positron operation. Examples of these are the vacuum and cooling-water systems.

The special phase shifters which can introduce an extra predetermined phase shift ($\approx 180^\circ$) on a pulse-to-pulse basis for positron acceleration are discussed in detail in Chapter 9.

16-6 Early positron operating experience (HDeS)

To date (July 1967) the positron beam has been set up about 15 times with an integrated operating time of about 150 hours at incident power levels up to about 40 kW. For the time being, it takes more time and effort to set up this beam than the usual electron beam, partly because the positron beam occupies a larger transverse phase space and adjustments are more critical. Customarily, the beam is tuned by sequentially optimizing the transmission near the radiator and empirically adjusting focusing and steering to maximize the positron current at the sector drift sections, using the same instrumentation as for the main electron beam. The intensity monitors (linear Q) work well at maximum positron intensity, but the RF position monitors operate very close to their thresholds of usefulness. From run to run, the optimum settings reproduce fairly well, but each time a final optimization is required to obtain the best beam. Tuning by using special intensity monitors within Sector 11 has not increased the final positron intensity. This procedure is complicated because, close to the source, there are still many particles inside the machine that are *not* useful positrons but which activate whatever detecting device is being used. After the positron beam is momentum analyzed, the amount of RF phase shift is finely tuned to get the best momentum spectrum.

Typically, the positron yield observed at the end of Sector 11 is 2 or 3% of the incident electron current (at 5 to 6 GeV). Of this, perhaps 75% is gradually lost as the beam is accelerated to Sector 20; from Sector 20 to the end of the machine the transmission is about 100%. About 30 to 50% of the beam leaving the accelerator proper goes through 1% (full-width) momentum slits, and spot sizes in the target area on the order of a few millimeters are common. This represents a specific yield of $1.5 \times 10^{-3} e^+/\text{GeV}$ of e^- and it corresponds to an average positron current of $0.15 \mu\text{A}$ for 100 kW incident on the radiator.

The positron yield as a function of RF phase shift shows a rather sharp peak near 165° ; hence, conceptually, the RF must be reversed in phase by exactly 180° and then retarded by 15° with respect to the positron beam being accelerated. Another peak of similar magnitude is obtained if the RF is

simply retarded by about 15° , which corresponds to relativistic positrons being decelerated, slipping in phase by about 180° , and then being captured and accelerated.¹⁹ The turning point occurs within the solenoid so that the particles are contained while their longitudinal velocities are low, and few positrons are lost. However, this mode of operation is not generally used because the beam energy is somewhat lower and the energy spread effects in the focusing system are worse.

The radiator is a source of electrons, as well as of positrons. The RF deflector system transmits only one particle or the other, which greatly simplifies the problem of beam monitoring. The deflector has been a useful and worthwhile part of the system. The best electron beam is 5–10 times greater than the best positron beam. If the system is tuned for positrons and then slight compromises are made to transmit electrons, the intensities are comparable. Under these conditions, the phase shifters in the first third of the accelerator and the steering dipole current in the RF deflector area must be switched on a pulse-to-pulse basis to select the sign of the accelerated beam.

Acknowledgments

J. Pine (Caltech) has been, and still is intimately involved in all phases of the positron system and has contributed many of the ideas that have been incorporated. J. Mar (Caltech) constructed much of the sensitive monitoring equipment used in the early tuning of the positron beam. A. L. Eldredge provided much counsel, direction, and stimulus. C. L. Rasmussen has overseen the materialization of numerous ideas and the rectification of a few bad ones. A. V. Lisin has contributed valuable criticism and advice.

References

- 1 D. Yount and J. Pine, *Nucl. Instr. Methods*, **15**, 45 (1962).
- 2 J. Pine in "1963 Summer Study Report," Rept. No. SLAC-25, Part I, Section D, Stanford Linear Accelerator Center, Stanford University, Stanford, California (January 1964).
- 3 C. D. Zerby and H. S. Moran, *J. Appl. Phys.* **34**, 2445 (1963).
- 4 J. Pine and H. DeStaebler, "Pulse Thermal Stresses in the Positron Radiator," Tech. Note No. SLAC-TN-66-31, Stanford Linear Accelerator Center, Stanford University, Stanford, California (July 1966). This note includes measurements of shower size with 1-GeV electrons incident on a layered radiator.
- 5 J. Pine and H. DeStaebler, "Heating Test of Positron Slug Radiator," Tech. Note No. SLAC-TN-67-18, Stanford Linear Accelerator Center, Stanford University, Stanford, California (June 1967).
- 6 T. L. Aggson and L. Burnod, "Production de positrons à l'accélérateur d'Orsay: détermination de la section efficace à 0° sur cibles épaisses." Rept. No. LAL-27, Laboratoire de l'Accélérateur Linéaire, Orsay, France (October 1962).

- 7 H. DeStaebler, "Remarks on Positron Intensities," Tech. Note No. SLAC-TN-65-23, Stanford Linear Accelerator Center, Stanford University, Stanford, California (March 1965).
- 8 P. A. Sturrock, *Static and Dynamic Electron Optics*, Cambridge Univ. Press, London and New York, 1965.
- 9 E. Ferlenghi and L. Mango, "Calcoli per L'Ottica di Trasporto dei Positroni nell'Acceleratore Lineare di Frascati," Rept. No. LNF-63/70, Laboratori Nazionali di Frascati, Rome, Italy (November 1963).
- 10 D. E. Lobb, "A Study of a Focusing System for Positron Beams," Rept. No. SAL-5 (Ph.D. Thesis), Saskatchewan Accelerator Laboratory, University of Saskatchewan, Saskatoon, Saskatchewan (March 1966).
- 11 C. S. Nunan, "A Positron Linear Accelerator Design," *IEEE Trans. Nucl. Sci.* NS-12, No. 3, p. 465 (June 1965).
- 12 H. Brechna, "Effect of Nuclear Radiation on Organic Materials; Specifically Magnet Insulation in High-Energy Accelerators," Rept. No. SLAC-40, Stanford Linear Accelerator Center, Stanford University, Stanford, California (March 1965).
- 13 H. Brechna, "Electromagnets for High Energy Physics Applications," in *Proc. Intern. Symposium Magnet Technol., Stanford Linear Accelerator Center, September 1967* (H. Brechna and H. S. Gordon, eds.), Conf-650922, p. 1, Clearinghouse for Federal Scientific and Technical Information, Springfield, Virginia.
- 14 F. C. Gunther, *Trans. Am. Soc. Mech. Engrs.* 73, 115-123 (1951).
- 15 H. Brechna and D. B. Montgomery, "A High Performance dc Magnet Utilizing Axial Cooled Discs," Rept. No. NML-62-1, p. 18, National Magnet Laboratory, Massachusetts Institute of Technology, Cambridge, Massachusetts (September 1962).
- 16 S. Mirshak, W. S. Durant, and R. H. Towell, "Heat Flux at Burnout," Rept. No. DP-355, Du Pont de Nemours (E.I.) and Co., Savannah River Laboratory, Augusta, Georgia.
- 17 Wm. McAdams, W. E. Kennel, C. S. Minden, R. Carl, P. M. Picornell, and J. E. Dew, *Ind. Eng. Chem.* 41, 1945-1953 (1949).
- 18 A technical description of the RF deflector is given in O. H. Altenmueller, R. R. Larsen, and G. A. Loew, *Rev. Sci. Instr.* 35, 436 (1964). A more detailed description of the whole deflection system is given in G. A. Loew and O. H. Altenmueller, "Design and Applications of RF Deflecting Structures at SLAC," in *Proc. Fifth Intern. Conf. on High-Energy Accelerators, Frascati, Italy, 1965*, pp. 551-553 (C.N.E.N., Rome, 1966).
- 19 The theory of capture in a traveling wave structure was developed by J. C. Slater, *Rev. Modern Phys.* 20, 473 (1948).

